A Comprehensive Analysis of Error Sources in Electronic Fully Digital Impedance Bridges

A Comprehensive Analysis of Error Sources in Electronic Fully Digital Impedance Bridges

Massimo Ortolano, Martina Marzano, Vincenzo D'Elia, Ngoc Thanh Mai Tran, Ryszard Rybski, *Member, IEEE*, Janusz Kaczmarek, *Member, IEEE*, Mirosław Kozioł, *Member, IEEE*, Krzysztof Musioł, Andreas Elmholdt Christensen, Luca Callegaro, Jan Kucera, and Oliver Power, *Member, IEEE*

***Abstract*— Fully digital impedance bridges are emerging as measuring instruments for primary electrical impedance metrology and the realization of impedance units and scales. This article presents a comprehensive analysis of electronic fully digital impedance bridges for both generating (based on digital-to-analog converters) and digitizing (based on analog-to-digital converters) bridges. The sources of measurement error are analyzed in detail and expressed by explicit mathematical formulas ready to be applied to the specific bridge and measurement case of interest. The same can be employed also as a basis to optimize the design and the operating parameters of digital bridges and evaluate the measurement uncertainty. A practical application of the analysis to the digital bridges developed and measurements performed in the framework of an international research project is presented.**

***Index Terms*— Bridge circuits, calibration, impedance measurement, measurement errors, measurement uncertainty.**

I. Introduction

IMPEDANCE bridges compare an impedance ratio to a reference ratio (see [1] for a comprehensive review). In general, they can be classified in several ways on the basis of: 1) the implemented impedance definition (*two-terminal pair*[1] or *four-terminal pair*); 2) the reference ratio quantity (*voltage ratio* or *current ratio*); 3) the bridge architecture (*digitally assisted*, if the reference ratio is mainly defined by a transformer, or *fully digital*, if the reference ratio is completely defined by a digital system); 4) the generator type (*electronic*, if the generator is based on digital electronics, or *Josephson*, if the generator is a programmable Josephson voltage standard or a Josephson arbitrary waveform synthesizer); and 5) the means used to establish the ratio reading (*generating*, *sourcing*, or *DAC-based*, if the reference ratio is determined by the settings of a digital signal generator, or *digitizing*, *sampling*, or *ADC-based*, if the reference ratio is determined from digitized samples).

From the first designs of the 1980s [2]–[6], electronic fully digital impedance bridges based on polyphase digital signal generators have emerged in recent years as measuring systems suitable for primary impedance metrology [1], [7]–[11]. With typical accuracies in the 10^{-6}–10^{-5} range, these kinds of bridges are not as accurate as traditional transformer-ratio bridges [10], [12], [13] or Josephson bridges [14]–[17] but can measure impedances across the whole complex plane and are characterized by affordable cost, short measuring time, and ease of operation. These features make them suitable for smaller national metrology institutes and calibration laboratories.

We present here a comprehensive analysis of the error sources in electronic fully digital bridges for generating (Sections II and III) and digitizing bridges (Sections IV and V). In particular, this work aims at collecting and expanding in a unified and general way some of the results that are scattered throughout the literature on fully digital impedance bridges (e.g., [8], [17], and [18]). A short summary was presented in [19]. The analysis of electronic generating bridges partially applies to Josephson bridges too. Finally, in Section VII, we present some experimental results about the error sources in a few bridge designs that are being developed within the framework of the project EMPIR 17RPT04 VersICaL: *A versatile impedance calibration laboratory based on digital impedance bridges* [20].

[1]We shall use the terms *terminal pair* and *port* interchangeably.

Manuscript received August 27, 2020; revised October 12, 2020; accepted October 16, 2020. Date of publication October 27, 2020; date of current version December 18, 2020. This work has been realized within the Joint Research Project 17RPT04 VersICaL: A versatile impedance calibration laboratory based on digital impedance bridges. This project has received funding from the EMPIR programme co-financed by the Participating States and from the European Union's Horizon 2020 research and innovation programme. The Associate Editor coordinating the review process was Yicheng Wang. *(Corresponding author: Massimo Ortolano.)*

Massimo Ortolano is with the Department of Electronics and Telecommunications, Politecnico di Torino, 10129 Turin, Italy, and also with the Istituto Nazionale di Ricerca Metrologica (INRIM), 10135 Turin, Italy (e-mail: massimo.ortolano@polito.it).

Martina Marzano, Vincenzo D'Elia, and Luca Callegaro are with the Istituto Nazionale di Ricerca Metrologica (INRIM), 10135 Turin, Italy.

Ngoc Thanh Mai Tran is with the Istituto Nazionale di Ricerca Metrologica (INRIM), 10135 Turin, Italy, and also with the Politecnico di Torino, 10129 Turin, Italy.

Ryszard Rybski, Janusz Kaczmarek, and Mirosław Kozioł are with the Institute of Metrology, Electronics and Computer Science, University of Zielona Góra (UZG), 65-246 Zielona Góra, Poland.

Krzysztof Musioł is with the Department of Measurement Science, Electronics and Control, Silesian University of Technology (SUT), 44-100 Gliwice, Poland.

Andreas Elmholdt Christensen is with Trescal A/S, 8600 Silkeborg, Denmark.

Jan Kucera is with the Czech Metrology Institute (CMI), 638 00 Brno, Czech Republic.

Oliver Power is with the National Standards Authority of Ireland (NSAI), Dublin 9, D09 A0E4, Ireland.

Digital Object Identifier 10.1109/TIM.2020.3034115

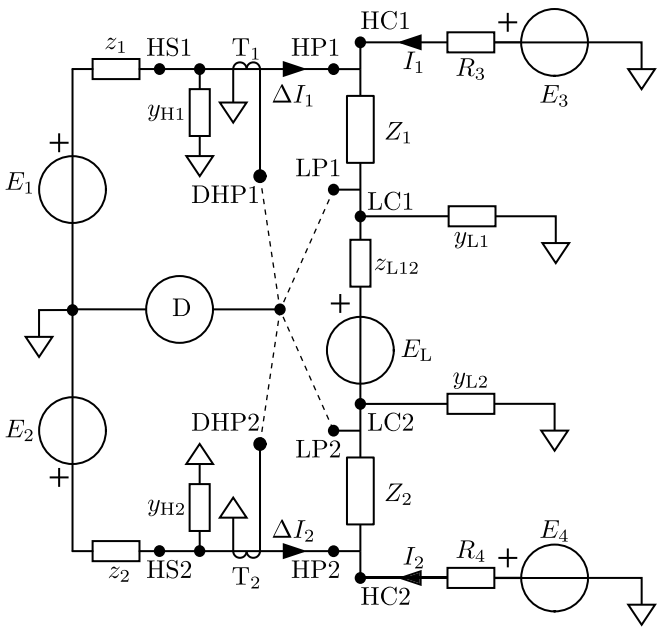

Fig. 1. Basic schematic of a typical four-terminal-pair fully digital generating impedance bridge. The relevant stray parameters are represented by small boxes designated by lower case symbols.

We remark that we shall consider only the errors caused by the bridge networks within the boundaries of the bridge ports and not those caused by the interconnections between the bridge ports and the impedances under measurement, their matching, and the imperfections of the impedances under measurement themselves. For the analysis of these error sources, see [21].

II. Generating Impedance Bridges

For the purpose of analyzing error sources, common four-terminal-pair fully digital generating impedance bridges can be reduced to the basic schematic of Fig. 1, omitting the shield conductor for readability.

The four-terminal-pair impedances under comparison are Z_1, connected to the bridge ports LC1, LP1, HC1 and HP1, and Z_2, connected to the bridge ports LC2, LP2, HC2, and HP2. The voltages[2] from E_1 to E_4 represent the output channels of a polyphase digital sinusoidal signal generator[3] operating at frequency f. The voltage E_L is usually applied by means of an injection transformer, not shown in the figure, whose primary winding is driven by another generator channel E_5. The bridge is operated to directly compare the impedance ratio Z_1/Z_2 to the main voltage ratio E_1/E_2. The auxiliary voltages E_3, E_4, and E_L realize the four-terminal-pair impedance definition: E_3 and E_4 generate, through the resistances R_3 and R_4, the currents I_1 and I_2 driving Z_1 and Z_2; E_L compensates for the voltage across the series impedance z_{L12} between the low potential ports LP1 and LP2 of Z_1 and Z_2, respectively.

The output impedances of E_1 and E_2 are represented by z_1 and z_2, respectively, including possible interconnection and additional series impedances.[4] The interconnection stray admittances between the channel outputs and ground are y_{H1} and y_{H2}. The stray admittances between the low-current ports of Z_1 and Z_2 and ground are y_{L1} and y_{L2}, respectively.

D represents a synchronous detector, typically a lock-in amplifier referenced to the operating frequency of the bridge. This detector can be connected, in turn, to the four detection ports LP1, LP2, DHP1, and DHP2 to check the bridge balance. The ports DHP1 and DHP2 are connected to the transformers T_1 and T_2, which can be operated either as current transformers or mutual inductors, to detect the residual currents ΔI_1 and ΔI_2. If D operates as a current detector, measuring the short circuit currents $I_{DHP1} = \Delta I_1/n$ and $I_{DHP2} = \Delta I_2/n$ at DHP1 and DHP2, respectively, T_1 and T_2 operate as current transformers with turns ratio n. If D operates as a voltage detector, measuring the open-circuit voltages $V_{DHP1} = Z_m \Delta I_1$ and $V_{DHP2} = Z_m \Delta I_2$, T_1 and T_2 operate as mutual inductors with mutual impedance Z_m.

The bridge is balanced, and the four-terminal-pair definition of the impedances is fulfilled when $V_{LP1} = V_{LP2} = 0$ and $\Delta I_1 = \Delta I_2 = 0$. The balance can be attained by adjusting, in magnitude and phase, the voltages from E_1 to E_4 and E_L (through E_5). The conditions $V_{LP1} = V_{LP2} = 0$ can be replaced by either $V_{LP1} = 0$ and $V_{LP1} - V_{LP2} = 0$, or $V_{LP1} + V_{LP2} = 0$ and $V_{LP1} - V_{LP2} = 0$. The condition $V_{LP1} - V_{LP2} = 0$ can be checked by using D as a differential detector between the ports LP1 and LP2.

When the bridge is balanced, neglecting the effect of the stray parameters (ideal bridge), the impedance ratio is given by

$$W = \frac{Z_1}{Z_2} = -\frac{E_1}{E_2}. \tag{1}$$

III. Error Sources in Generating Bridges

In a generating bridge, the readings E_1^{read} and E_2^{read} of the voltage phasors E_1 and E_2 are usually computed from the samples synthesizing the two waveforms. To cancel the effect of the generator gain error (Section III-A), the bridge reading is obtained from two successive balances, with *channel* or *impedance swapping*. The bridge is first balanced as in Fig. 1 (*forward* configuration)[5] and then with the two main channels or the two impedances exchanged (*reverse* configuration). The reverse configuration can be obtained by either swapping: 1) the bridge arms at the ports HP1 and HP2; 2) the channels

[2]In the following, quantity symbols labeling voltages and currents represent complex phasors associated with voltage and current signals. The symbols from E_1 to E_5 represent both the generator channels and the phasors associated with their output voltages.

[3]Digital signal generators employed in digital bridges can be based either on direct digital synthesizers (DDSs) with phase accumulation (e.g., [22]) or on synthesizers with variable sample rate (e.g., [23]). The former allow fine and agile frequency control and phase continuous operation; the latter allow better control and predictability of the spectrum of the generated signal (see [24] for more details on digital waveform generators). The two generation techniques can also be combined.

[4]Resistors, typically in the 10 Ω range, may need to be added in series to the output channels to isolate the output amplifiers from large capacitive loads and preventing self-oscillations [25, Sec. 8.4].

[5]Equivalent terms found in the literature are *exchange* or *inversion* instead of *swapping* and *direct* instead of *forward*.

E_1 and E_2 at the ports HS1 and HS2; or 3) the impedances Z_1 and Z_2 at their respective ports. Cases 1) and 2) minimize the number of switched ports but modify the bridge network between the two configurations, whereas case 3) does not change the bridge network but requires the switching of more ports.

The bridge reading is computed as

$$W^{\text{read}} = \sqrt{W_{\text{F}}^{\text{read}} W_{\text{R}}^{\text{read}}} \tag{2}$$

with

$$W_{\text{F}}^{\text{read}} = -\frac{E_{1\text{F}}^{\text{read}}}{E_{2\text{F}}^{\text{read}}} \tag{3}$$

and

$$W_{\text{R}}^{\text{read}} = -\frac{E_{2\text{R}}^{\text{read}}}{E_{1\text{R}}^{\text{read}}} \tag{4}$$

where the quantities labeled with the F subscript refer to the balance in the forward configuration and those labeled with the R subscript refer to the balance in the reverse configuration. The square root of (2), with complex argument, should be determined so that the phase of W^{read} agrees with that of W (or with that of either $W_{\text{F}}^{\text{read}}$ or $W_{\text{R}}^{\text{read}}$). Alternatively, following [17], (2) can be rewritten as

$$W^{\text{read}} = W_{\text{F}}^{\text{read}} \sqrt{\frac{W_{\text{R}}^{\text{read}}}{W_{\text{F}}^{\text{read}}}} \tag{5}$$

where, now, since $W_{\text{F}}^{\text{read}} \approx W_{\text{R}}^{\text{read}}$, the square root should be determined with positive real part. The advantage of (5) with respect to (2) is that, in the former, the square root can be determined without any reference to the unknown W.

The impedance ratio W differs from W^{read} by the error $\Delta W = W^{\text{read}} - W$. The main components of this error are: 1) the *generator nonlinearity* error ΔW^{nl} (Section III-A); 2) the *generator crosstalk* error ΔW^{ct} (Section III-B); 3) the *generator loading* error ΔW^{ld} (Section III-C); and 4) the *bridge unbalance* errors ΔW^{lb} and ΔW^{hb} (Sections III-D and III-E, respectively).

From (2)

$$\frac{\Delta W}{W^{\text{read}}} \approx \frac{1}{2}\left(\frac{\Delta W_{\text{F}}}{W_{\text{F}}^{\text{read}}} + \frac{\Delta W_{\text{R}}}{W_{\text{R}}^{\text{read}}}\right) \tag{6}$$

with $\Delta W_{\text{F}} = W_{\text{F}}^{\text{read}} - W$ and $\Delta W_{\text{R}} = W_{\text{R}}^{\text{read}} - W$. Equation (6) will be used in Sections III-A–III-E to determine ΔW by combining the individual errors of the forward and reverse measurements. All the approximations made in the derivations of Sections III-A–III-E are at first order with respect to the perturbing parameters; the second-order terms are negligible with respect to the typical bridge accuracies stated in Section I.

A. Generator Nonlinearity

Due to the generator nonidealities, the actual voltage phasors differ from the readings, $E_{k\text{X}} = [1 + g_k(E_{k\text{X}}^{\text{read}})]E_{k\text{X}}^{\text{read}}$, $k = 1, 2$ and $\text{X} = \text{F}, \text{R}$, with $g_k(E_{k\text{X}}^{\text{read}})$ representing a possibly voltage-dependent complex gain error that accounts for nonlinear magnitude and phase errors [8]. Assuming $|g_k(E_{k\text{X}})| \ll 1$, from (3) and (4), $\Delta W_{\text{F}}^{\text{nl}}/W_{\text{F}}^{\text{read}} \approx g_2(E_{2\text{F}}^{\text{read}}) - g_1(E_{1\text{F}}^{\text{read}})$ and $\Delta W_{\text{R}}^{\text{nl}}/W_{\text{R}}^{\text{read}} \approx g_1(E_{1\text{R}}^{\text{read}}) - g_2(E_{2\text{R}}^{\text{read}})$. Combining these with (6) yields

$$\frac{\Delta W^{\text{nl}}}{W^{\text{read}}} \approx -\frac{1}{2}\big[g_1\big(E_{1\text{F}}^{\text{read}}\big) - g_1\big(E_{1\text{R}}^{\text{read}}\big) - g_2\big(E_{2\text{F}}^{\text{read}}\big) + g_2\big(E_{2\text{R}}^{\text{read}}\big)\big]. \tag{7}$$

From (7), if the generator were perfectly linear, that is, if the gain errors $g_k(E_{k\text{X}}^{\text{read}})$ were independent of the generated voltages, then ΔW^{nl} would be zero. In practice, suppose that Z_1 is a reference impedance and that one fixes $E_{2\text{R}}^{\text{read}} = E_{1\text{F}}^{\text{read}}$ so that the bridge current is the same in the forward and reverse configurations. In this case, taking into account (3) and (4), we can rewrite (7) as

$$\frac{\Delta W^{\text{nl}}}{W^{\text{read}}} \approx -\frac{1}{2}\big[g_1\big(E_{1\text{F}}^{\text{read}}\big) - g_1\big(-E_{1\text{F}}^{\text{read}}/W_{\text{R}}^{\text{read}}\big) - g_2\big(-E_{1\text{F}}^{\text{read}}/W_{\text{F}}^{\text{read}}\big) + g_2\big(E_{1\text{F}}^{\text{read}}\big)\big] \tag{8}$$

or

$$\frac{\Delta W^{\text{nl}}}{W^{\text{read}}} \approx -\frac{1}{2}\big[\Delta g_1\big(E_{1\text{F}}^{\text{read}}, -W_{\text{R}}^{\text{read}}\big) + \Delta g_2\big(E_{1\text{F}}^{\text{read}}, -W_{\text{F}}^{\text{read}}\big)\big] \tag{9}$$

having defined

$$\Delta g_k\big(E_{k\text{X}}^{\text{read}}, W\big) = g_k\big(E_{k\text{X}}^{\text{read}}\big) - g_k\big(E_{k\text{X}}^{\text{read}}/W\big). \tag{10}$$

When $|W_{\text{F}}^{\text{read}}| \approx |W_{\text{R}}^{\text{read}}| \approx |W| \approx 1$, we can expect, from the above equation, a partial cancellation of the individual error terms, depending on the differential nonlinearity of the generator, yielding a minimum of $|\Delta W^{\text{nl}}/W^{\text{read}}|$. When the ratio magnitude is large, instead, we can expect an increase of $|\Delta W^{\text{nl}}/W^{\text{read}}|$, mainly dependent on the integral nonlinearity of the generator.

B. Generator Crosstalk

Due to electric, magnetic, or common impedance coupling [26], each channel of the generator can interfere with the others. We can, therefore, write, with the notation for k and X introduced in Section III-A

$$E_{k\text{X}} = E_{k\text{X}}^{\text{read}} + E_{k0} + \sum_{\substack{j=1\\ j\neq k}}^{5} a_{kj} E_{j\text{X}}^{\text{read}} \tag{11}$$

where the term E_{k0} represents a possible residual voltage at the channel output, independent of the other channels settings, and a_{kj} is the (complex) coupling coefficient from channel j to channel k.

Substituting (11) into (3) and (4), combining the forward and reverse errors with (6), and approximating at first order in the E_{k0}'s and a_{kj}'s yield

$$\frac{\Delta W^{\text{ct}}}{W^{\text{read}}} \approx -\frac{1}{2}\sum_{k=1}^{2} E_{k0}\left(\frac{1}{E_{k\text{F}}^{\text{read}}} - \frac{1}{E_{k\text{R}}^{\text{read}}}\right) - \frac{1}{2}\sum_{k=1}^{2}\sum_{\substack{j=1\\ j\neq k}}^{5} a_{kj}\left(\frac{E_{j\text{F}}^{\text{read}}}{E_{k\text{F}}^{\text{read}}} - \frac{E_{j\text{R}}^{\text{read}}}{E_{k\text{R}}^{\text{read}}}\right). \tag{12}$$

By pulling out from the sum the terms with $j = 1, 2$, we can rewrite (12) as

$$\frac{\Delta W^{\mathrm{ct}}}{W^{\mathrm{read}}} \approx -\frac{1}{2}\sum_{k=1}^{2} E_{k0}\left(\frac{1}{E_{k\mathrm{F}}^{\mathrm{read}}} - \frac{1}{E_{k\mathrm{R}}^{\mathrm{read}}}\right) - \frac{1}{2}a_{12}\left(W_{\mathrm{R}}^{\mathrm{read}} - \frac{1}{W_{\mathrm{F}}^{\mathrm{read}}}\right) - \frac{1}{2}a_{21}\left(\frac{1}{W_{\mathrm{R}}^{\mathrm{read}}} - W_{\mathrm{F}}^{\mathrm{read}}\right) - \frac{1}{2}\sum_{k=1}^{2}\sum_{\substack{j=3\\ j\neq k}}^{5} a_{kj}\left(\frac{E_{j\mathrm{F}}^{\mathrm{read}}}{E_{k\mathrm{F}}^{\mathrm{read}}} - \frac{E_{j\mathrm{R}}^{\mathrm{read}}}{E_{k\mathrm{R}}^{\mathrm{read}}}\right). \tag{13}$$

There is, thus, a partial cancellation of the terms in a_{12} and a_{21} when $W \approx \pm 1$.

C. Generator Loading

The admittances y_{H1} and y_{H2} load the channels E_1 and E_2 causing voltage drops across the output impedances z_1 and z_2. This can be assimilated to a gain error and its effect on the measurement estimated as in Section III-A.

If the exchange from the forward to the reverse configuration is done at the ports HP1 and HP2, as in cases 1) and 3) of Section II, then

$$E_{k\mathrm{X}} = \frac{E_{k\mathrm{X}}^{\mathrm{read}}}{1 + z_k y_{\mathrm{H}k}} \approx (1 - z_k y_{\mathrm{H}k}) E_{k\mathrm{X}}^{\mathrm{read}}. \tag{14}$$

The equivalent gain error is $g_k = -z_k y_{\mathrm{H}k}$, independent of the generated voltages: from (7), the resulting generator loading error ΔW^{ld} is, therefore, zero.

If, instead, the channels are exchanged at the ports HS1 and HS2, as in case 2) of Section II, then

$$E_{k\mathrm{F}} = \frac{E_{k\mathrm{F}}^{\mathrm{read}}}{1 + z_k y_{\mathrm{H}k}} \approx (1 - z_k y_{\mathrm{H}k}) E_{k\mathrm{F}}^{\mathrm{read}} \tag{15}$$

$$E_{1\mathrm{R}} = \frac{E_{1\mathrm{R}}^{\mathrm{read}}}{1 + z_1 y_{\mathrm{H2}}} \approx (1 - z_1 y_{\mathrm{H2}}) E_{1\mathrm{R}}^{\mathrm{read}} \tag{16}$$

and

$$E_{2\mathrm{R}} = \frac{E_{2\mathrm{R}}^{\mathrm{read}}}{1 + z_2 y_{\mathrm{H1}}} \approx (1 - z_2 y_{\mathrm{H1}}) E_{2\mathrm{R}}^{\mathrm{read}}. \tag{17}$$

From (7), with $g_k(E_{k\mathrm{F}}^{\mathrm{read}}) = -z_k y_{\mathrm{H}k}$, $g_1(E_{1\mathrm{R}}^{\mathrm{read}}) = -z_1 y_{\mathrm{H2}}$, and $g_2(E_{2\mathrm{R}}^{\mathrm{read}}) = -z_2 y_{\mathrm{H1}}$, the resulting generator loading error is

$$\frac{\Delta W^{\mathrm{ld}}}{W^{\mathrm{read}}} \approx \frac{1}{2}(z_1 + z_2)(y_{\mathrm{H1}} - y_{\mathrm{H2}}). \tag{18}$$

The generator loading error is minimized by a symmetric construction, for which $y_{\mathrm{H1}} \approx y_{\mathrm{H2}}$. Furthermore, if z_1 and z_2 are mainly resistive and y_{H1} and y_{H2} are mainly capacitive, as it happens at low frequency, the error is at first order on the phase of W and at second order on its magnitude. Equation (18) can be also adapted to two-terminal-pair bridges [8].

D. Low Unbalance

If the bridge is imperfectly balanced with $V_{\mathrm{LP1}} \neq 0$ and $V_{\mathrm{LP2}} \neq 0$, two issues arise. First, the voltages across the impedances Z_1 and Z_2 differ from E_1 and E_2. Second, the currents crossing Z_1 and Z_2 are no longer equal because some current is drawn through the stray admittances y_{L1} and y_{L2}.

All other error sources neglected, writing Kirchhoff's current law at terminals LP1 and LP2 for the forward configuration yields

$$(Y_1 + y_{\mathrm{L1}})V_{\mathrm{LP1F}} - Y_1 E_{1\mathrm{F}}^{\mathrm{read}} - y_{\mathrm{L12}}\left(V_{\mathrm{LP2F}} - V_{\mathrm{LP1F}} + E_{\mathrm{LF}}^{\mathrm{read}}\right) = 0 \tag{19}$$

$$(Y_2 + y_{\mathrm{L2}})V_{\mathrm{LP2F}} - Y_2 E_{2\mathrm{F}}^{\mathrm{read}} - y_{\mathrm{L12}}\left(V_{\mathrm{LP1F}} - V_{\mathrm{LP2F}} - E_{\mathrm{LF}}^{\mathrm{read}}\right) = 0 \tag{20}$$

with $Y_1 = 1/Z_1$, $Y_2 = 1/Z_2$, and $y_{\mathrm{L12}} = 1/z_{\mathrm{L12}}$. Adding the two above equations cancels the last term

$$(Y_1 + y_{\mathrm{L1}})V_{\mathrm{LP1F}} + (Y_2 + y_{\mathrm{L2}})V_{\mathrm{LP2F}} - Y_1 E_{1\mathrm{F}}^{\mathrm{read}} - Y_2 E_{2\mathrm{F}}^{\mathrm{read}} = 0. \tag{21}$$

By defining the *common mode voltage* (or *Wagner voltage*) $V_{\mathrm{LPF}} = (V_{\mathrm{LP1F}} + V_{\mathrm{LP2F}})/2$ and the *differential voltage* (or *Kelvin voltage*) $\Delta V_{\mathrm{LPF}} = V_{\mathrm{LP1F}} - V_{\mathrm{LP2F}}$, we can rewrite (21) as

$$(Y_1 + Y_2 + y_{\mathrm{L1}} + y_{\mathrm{L2}})V_{\mathrm{LPF}} + (Y_1 - Y_2 + y_{\mathrm{L1}} - y_{\mathrm{L2}})\frac{\Delta V_{\mathrm{LPF}}}{2} - Y_1 E_{1\mathrm{F}}^{\mathrm{read}} - Y_2 E_{2\mathrm{F}}^{\mathrm{read}} = 0. \tag{22}$$

Solving (22) for $Y_2 E_{2\mathrm{F}}^{\mathrm{read}}$ allows us to write

$$W = \frac{Y_2}{Y_1} = \frac{Y_2 E_{2\mathrm{F}}^{\mathrm{read}}}{Y_1 E_{2\mathrm{F}}^{\mathrm{read}}} \tag{23}$$

$$= -\frac{E_{1\mathrm{F}}^{\mathrm{read}}}{E_{2\mathrm{F}}^{\mathrm{read}}} + \frac{(Y_1 + Y_2 + y_{\mathrm{L1}} + y_{\mathrm{L2}})V_{\mathrm{LPF}}}{Y_1 E_{2\mathrm{F}}^{\mathrm{read}}} + \frac{(Y_1 - Y_2 + y_{\mathrm{L1}} - y_{\mathrm{L2}})\Delta V_{\mathrm{LPF}}}{2Y_1 E_{2\mathrm{F}}^{\mathrm{read}}} \tag{24}$$

from which

$$\frac{\Delta W_{\mathrm{F}}^{\mathrm{lb}}}{W_{\mathrm{F}}^{\mathrm{read}}} = \frac{(Y_1 + Y_2 + y_{\mathrm{L1}} + y_{\mathrm{L2}})V_{\mathrm{LPF}}}{Y_1 E_{1\mathrm{F}}^{\mathrm{read}}} + \frac{(Y_1 - Y_2 + y_{\mathrm{L1}} - y_{\mathrm{L2}})\Delta V_{\mathrm{LPF}}}{2Y_1 E_{1\mathrm{F}}^{\mathrm{read}}} \tag{25}$$

$$= \left(1 + W + \frac{y_{\mathrm{L1}} + y_{\mathrm{L2}}}{Y_1}\right)\frac{V_{\mathrm{LPF}}}{E_{1\mathrm{F}}^{\mathrm{read}}} + \left(1 - W + \frac{y_{\mathrm{L1}} - y_{\mathrm{L2}}}{Y_1}\right)\frac{\Delta V_{\mathrm{LPF}}}{2E_{1\mathrm{F}}^{\mathrm{read}}}. \tag{26}$$

For the reverse configuration, for cases 1) and 2) of Section III, we can exchange E_1 and E_2 in (22) and repeat the foregoing steps to obtain

$$\frac{\Delta W_{\mathrm{R}}^{\mathrm{lb}}}{W_{\mathrm{R}}^{\mathrm{read}}} = \left(1 + W + \frac{y_{\mathrm{L1}} + y_{\mathrm{L2}}}{Y_1}\right)\frac{V_{\mathrm{LPR}}}{E_{2\mathrm{R}}^{\mathrm{read}}} + \left(1 - W + \frac{y_{\mathrm{L1}} - y_{\mathrm{L2}}}{Y_1}\right)\frac{\Delta V_{\mathrm{LPR}}}{2E_{2\mathrm{R}}^{\mathrm{read}}}. \tag{27}$$

This, combined with (26) through (6), finally yields

$$\frac{\Delta W^{\mathrm{lb}}}{W^{\mathrm{read}}} = \frac{1}{2}\left(1 + W + \frac{y_{\mathrm{L1}} + y_{\mathrm{L2}}}{Y_1}\right)\left(\frac{V_{\mathrm{LPF}}}{E_{1\mathrm{F}}^{\mathrm{read}}} + \frac{V_{\mathrm{LPR}}}{E_{2\mathrm{R}}^{\mathrm{read}}}\right) + \frac{1}{4}\left(1 - W + \frac{y_{\mathrm{L1}} - y_{\mathrm{L2}}}{Y_1}\right)\left(\frac{\Delta V_{\mathrm{LPF}}}{E_{1\mathrm{F}}^{\mathrm{read}}} + \frac{\Delta V_{\mathrm{LPR}}}{E_{2\mathrm{R}}^{\mathrm{read}}}\right). \tag{28}$$

For case 3), we can instead exchange Y_1 and Y_2 in (22) to obtain

$$\frac{\Delta W^{\mathrm{lb}}}{W^{\mathrm{read}}} = \frac{1}{2}\left(1 + W + \frac{y_{\mathrm{L1}} + y_{\mathrm{L2}}}{Y_1}\right)\left(\frac{V_{\mathrm{LPF}}}{E_{1\mathrm{F}}^{\mathrm{read}}} + \frac{V_{\mathrm{LPR}}}{E_{2\mathrm{R}}^{\mathrm{read}}}\right) + \frac{1}{4}\left(W - 1 + \frac{y_{\mathrm{L1}} - y_{\mathrm{L2}}}{Y_1}\right)\left(\frac{\Delta V_{\mathrm{LPF}}}{E_{1\mathrm{F}}^{\mathrm{read}}} + \frac{\Delta V_{\mathrm{LPR}}}{E_{2\mathrm{R}}^{\mathrm{read}}}\right). \tag{29}$$

The specific forms of (28) and (29) have been chosen according to the idea, as laid down in Section III-A, that Z_1 is a reference impedance and that one typically works with $E_{1\mathrm{F}}^{\mathrm{read}} = E_{2\mathrm{R}}^{\mathrm{read}}$ so that the same current circulates in the bridge in the forward and reverse configurations. For fixed $E_{1\mathrm{F}}^{\mathrm{read}} = E_{2\mathrm{R}}^{\mathrm{read}}$, the voltage across Z_2 is inversely proportional to W, such that the magnitude of $|\Delta W^{\mathrm{lb}}/W^{\mathrm{read}}|$ increases with W as the relative effect of the unbalance at the low potential ports. From (28) and (29), the error is reduced by a symmetric construction with $y_{\mathrm{L1}} \approx y_{\mathrm{L2}}$ and when operating at $W \approx \pm 1$.

E. High Unbalance

If the bridge is imperfectly balanced with $\Delta I_1 \neq 0$ and $\Delta I_2 \neq 0$, the voltage drops across z_1 and z_2 generate a measurement error.

Let $\Delta I_{k\mathrm{X}}$ be the residual current crossing z_k at the forward and reverse balances. Then

$$E_{k\mathrm{X}} = E_{k\mathrm{X}}^{\mathrm{read}} - z_k \Delta I_{k\mathrm{X}}. \tag{30}$$

From (3), (4), (6), and (30) and approximating at first order in the products $z_k \Delta I_{k\mathrm{X}}$, we get

$$\frac{\Delta W^{\mathrm{hb}}}{W^{\mathrm{read}}} \approx \frac{1}{2}\left(\frac{z_1 \Delta I_{1\mathrm{F}}}{E_{1\mathrm{F}}^{\mathrm{read}}} - \frac{z_2 \Delta I_{2\mathrm{F}}}{E_{2\mathrm{F}}^{\mathrm{read}}} - \frac{z_1 \Delta I_{1\mathrm{R}}}{E_{1\mathrm{R}}^{\mathrm{read}}} + \frac{z_2 \Delta I_{2\mathrm{R}}}{E_{2\mathrm{R}}^{\mathrm{read}}}\right). \tag{31}$$

Recalling the description of Section III-E, if D is a current detector and T_1 and T_2 current transformers with turns ratio n, we can rewrite (31) as

$$\frac{\Delta W^{\mathrm{hb}}}{W^{\mathrm{read}}} \approx \frac{n}{2}\left(\frac{z_1 I_{\mathrm{DHP1F}}}{E_{1\mathrm{F}}^{\mathrm{read}}} - \frac{z_2 I_{\mathrm{DHP2F}}}{E_{2\mathrm{F}}^{\mathrm{read}}} - \frac{z_1 I_{\mathrm{DHP1R}}}{E_{1\mathrm{R}}^{\mathrm{read}}} + \frac{z_2 I_{\mathrm{DHP2R}}}{E_{2\mathrm{R}}^{\mathrm{read}}}\right) \tag{32}$$

with $I_{\mathrm{DHP}k\mathrm{X}}$'s representing the residual currents detected by D at the secondary windings of T_1 and T_2 in the forward and reverse balances. If, instead, D is a voltage detector and T_1 and T_2 mutual inductors with mutual impedance Z_{m}, we can rewrite (31) as

$$\frac{\Delta W^{\mathrm{hb}}}{W^{\mathrm{read}}} \approx \frac{1}{2Z_{\mathrm{m}}}\left(\frac{z_1 V_{\mathrm{DHP1F}}}{E_{1\mathrm{F}}^{\mathrm{read}}} - \frac{z_2 V_{\mathrm{DHP2F}}}{E_{2\mathrm{F}}^{\mathrm{read}}} - \frac{z_1 V_{\mathrm{DHP1R}}}{E_{1\mathrm{R}}^{\mathrm{read}}} + \frac{z_2 V_{\mathrm{DHP2R}}}{E_{2\mathrm{R}}^{\mathrm{read}}}\right) \tag{33}$$

with $V_{\mathrm{DHP}k\mathrm{X}}$'s representing the residual voltages detected by D at the secondary windings of T_1 and T_2 in the forward and reverse balances.

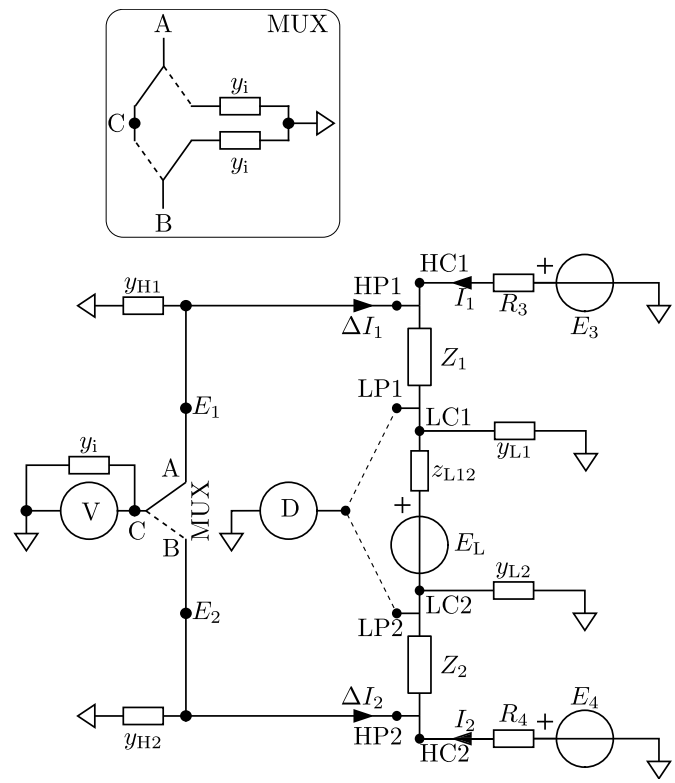

Fig. 2. Basic schematic of a typical four-terminal-pair fully digital digitizing impedance bridge. The relevant stray parameters are represented by small boxes designated by lower case symbols. The top inset represents a common implementation of the multiplexer MUX with two switches.

IV. Digitizing Impedance Bridges

The network of a typical digitizing bridge with the relevant stray parameters is represented in Fig. 2. Corresponding symbols are defined as in Section II. V represents a digitizer with input admittance y_{i}. The element MUX, with ports A, B, and C, represents a multiplexer alternatively connecting the digitizer to the high-potential ports HP1 and HP2 of Z_1 and Z_2. The top inset represents a common implementation of the multiplexer MUX with two switches and two dummy impedances matched to y_{i}. The purpose of this arrangement is to keep the load on HP1 and HP2 independent of the MUX position. The interconnection admittances y_{H1} and y_{H2} at HP1 and HP2 can be reduced by using high-impedance buffers either at these ports or at the digitizer input [7], [27].

The bridge is balanced when $V_{\mathrm{LP1}} = V_{\mathrm{LP2}} = 0$, a condition that is detected by detector D, and the balance is attained by adjusting either E_3 or E_4 and E_{L}. The readings E_1^{read} and E_2^{read} of the voltage phasors E_1 and E_2 are computed from the samples recorded by the digitizer V. The digitizer is based on an analog-to-digital converter (ADC) whose clock is typically locked to the bridge operating frequency f. The detector D and the digitizer V can be actually the same device.

For an ideal digitizing bridge, the impedance ratio is given by (1).

V. Error Sources in Digitizing Bridges

Equations similar to those reported in Section III can be derived also for the error sources of a digitizing bridge, just by reinterpreting the meaning of some bridge parts.

Since the voltages across Z_1 and Z_2 are measured by the same digitizer, channel swapping may not be needed in this kind of bridge. However, channel swapping can still be used to cancel the effect of possible gain mismatches when buffers are present at HP1 and HP2. In the former case, the bridge reading is given by (3), in the latter, by (2).

The main components of the measurement error in digitizing bridges are: 1) the *digitizer nonlinearity* error ΔW^{nl} (Section V-A); 2) the *multiplexer switching* error ΔW^{sw} (Section V-B); and 3) the *bridge low unbalance* error ΔW^{lb} (Section V-C). Coherently with the analysis of Section III, all the approximations made in the derivations of Sections V-A–V-C are at first order with respect to the perturbing parameters; also in this case, the second-order terms are negligible with respect to the typical bridge accuracies stated in Section I.

A. Digitizer Nonlinearity

In this type of bridge, the actual voltages differ from the readings due to the digitizer nonidealities, instead of the generator nonidealities introduced in Section III-A.

Without channel swapping, representing the digitizer nonlinearity as $E_k = [1 + g(E_k^{\mathrm{read}})]E_k^{\mathrm{read}}$, we get

$$\frac{\Delta W^{\mathrm{nl}}}{W^{\mathrm{read}}} \approx g\left(E_2^{\mathrm{read}}\right) - g\left(E_1^{\mathrm{read}}\right). \tag{34}$$

With channel swapping, assuming different gains for the two channels of the digitizer, (7) holds again.

B. Multiplexer Switching

The usage of just one digitizer in the bridge requires a multiplexer (MUX in Fig. 2) to switch the digitizer input between different measurement ports. As pointed out in Section IV, the multiplexer is commonly designed to provide a constant load at its ports, independent of the multiplexer position. In a real construction, when the multiplexer switches, there will always be a small change of the load at its ports, and there will always be some crosstalk between the channels, typically caused by capacitive coupling. These imperfections in the multiplexer construction cause a measurement error because they change the bridge balance between the two positions.

Let us assume that the bridge is balanced, with $V_{\mathrm{LP1A}} = V_{\mathrm{LP2A}} = 0$ when MUX is in position A, and let $E_{1\mathrm{A}} = E_1^{\mathrm{read}}$ and $E_{2\mathrm{A}}$ be the voltages at HP1 and HP2, coinciding, in this case, with the voltages across Z_1 and Z_2, respectively. We can, therefore, write

$$W = -\frac{E_{1\mathrm{A}}}{E_{2\mathrm{A}}} = -\frac{E_1^{\mathrm{read}}}{E_{2\mathrm{A}}}. \tag{35}$$

When MUX is switched to position B, the currents ΔI_1 and ΔI_2 change because of its residual asymmetries. The bridge is, therefore, no longer perfectly balanced, the digitizer measures the voltage $E_{2\mathrm{B}} = E_2^{\mathrm{read}} \neq E_{2\mathrm{A}}$, the voltage at the low potential port of Z_2 is $V_{\mathrm{LP2B}} \neq 0$, and the voltage across Z_2 is $E_2^{\mathrm{read}} - V_{\mathrm{LP2B}}$. Let, in this case, assuming that V_{LP2B} is also recorded

$$W^{\mathrm{read}} = -\frac{E_1^{\mathrm{read}}}{E_2^{\mathrm{read}} - V_{\mathrm{LP2B}}} \tag{36}$$

the measurement error is then

$$\frac{\Delta W^{\mathrm{sw}}}{W^{\mathrm{read}}} \approx \frac{E_{2\mathrm{A}} - \left(E_2^{\mathrm{read}} - V_{\mathrm{LP2B}}\right)}{E_2^{\mathrm{read}}}. \tag{37}$$

By superposition

$$E_{2\mathrm{A}} = \frac{Z_2}{R_4 + Z_2}E_4 + (R_4 \,||\, Z_2)\Delta I_{2\mathrm{A}} \tag{38}$$

where $R_4 \,||\, Z_2$ is the parallel impedance between R_4 and Z_2, and $\Delta I_{2\mathrm{A}}$ is the current entering HP2. When MUX is switched to position B

$$E_2^{\mathrm{read}} = \frac{R_4}{R_4 + Z_2}V_{\mathrm{LP2B}} + \frac{Z_2}{R_4 + Z_2}E_4 + (R_4 \,||\, Z_2)\Delta I_{2\mathrm{B}}. \tag{39}$$

From (37)–(39), we obtain

$$\frac{\Delta W^{\mathrm{sw}}}{W^{\mathrm{read}}} \approx (R_4 \,||\, Z_2)\frac{\Delta I_{2\mathrm{A}} - \Delta I_{2\mathrm{B}}}{E_2^{\mathrm{read}}} + \frac{Z_2}{R_4 + Z_2}\frac{V_{\mathrm{LP2B}}}{E_2^{\mathrm{read}}}. \tag{40}$$

Furthermore, it can be shown by superposition that

$$V_{\mathrm{LP2B}} \approx -\frac{R_3(R_4 + Z_2)}{R_3 + Z_1 + R_4 + Z_2}(\Delta I_{1\mathrm{A}} - \Delta I_{1\mathrm{B}}) - \frac{R_4(R_3 + Z_1)}{R_3 + Z_1 + R_4 + Z_2}(\Delta I_{2\mathrm{A}} - \Delta I_{2\mathrm{B}}). \tag{41}$$

Substituting (41) into (40) yields

$$\frac{\Delta W^{\mathrm{sw}}}{W^{\mathrm{read}}} \approx -\frac{R_3 Z_2}{R_3 + Z_1 + R_4 + Z_2}\frac{\Delta I_{1\mathrm{A}} - \Delta I_{1\mathrm{B}}}{E_2^{\mathrm{read}}} + \frac{R_4 Z_2}{R_3 + Z_1 + R_4 + Z_2}\frac{\Delta I_{2\mathrm{A}} - \Delta I_{2\mathrm{B}}}{E_2^{\mathrm{read}}} \tag{42}$$

To determine the current difference $\Delta I_{1\mathrm{A}} - \Delta I_{1\mathrm{B}}$, we can refer to the multiplexer implementation represented in the inset of Fig. 2. When MUX is in position A, HP1 is loaded by y_{H1} and $y_{\mathrm{i}} + \Delta y_{\mathrm{iAA}}$, where the latter represents the MUX input admittance at port A when MUX is in position A, possibly differing from y_{i} by Δy_{iAA}. We can, therefore, write

$$\Delta I_{1\mathrm{A}} = -(y_{\mathrm{H1}} + y_{\mathrm{i}} + \Delta y_{\mathrm{iAA}})E_1^{\mathrm{read}} - \left(E_1^{\mathrm{read}} - E_{2\mathrm{A}}\right)y_{\mathrm{CB}} \tag{43}$$

where y_{CB} is the stray admittance between ports C and B when MUX is in position A (not shown in Fig. 2 to avoid cluttering the schematic). When MUX is in position B, HP1 is loaded by y_{H1} and $y_{\mathrm{i}} + \Delta y_{\mathrm{iAB}}$, where the latter represents the MUX input admittance at port A when MUX is in position B. We can, therefore, write

$$\Delta I_{1\mathrm{B}} = -(y_{\mathrm{H1}} + y_{\mathrm{i}} + \Delta y_{\mathrm{iAB}})E_{1\mathrm{B}} - \left(E_{1\mathrm{B}} - E_2^{\mathrm{read}}\right)y_{\mathrm{ac}} \tag{44}$$

where y_{ac} is the stray admittance between ports A and C when MUX is in position B. Subtracting (44) from (43) and taking into account that $E_{1\mathrm{B}} \approx E_{1\mathrm{A}} = E_1^{\mathrm{read}}$ and $E_{2\mathrm{A}} \approx E_{2\mathrm{B}} = E_2^{\mathrm{read}}$

$$\frac{\Delta I_{1\mathrm{A}} - \Delta I_{1\mathrm{B}}}{E_2^{\mathrm{read}}} \approx (\Delta y_{\mathrm{iAA}} - \Delta y_{\mathrm{iAB}})W^{\mathrm{read}} + (W^{\mathrm{read}} + 1)(y_{\mathrm{CB}} - y_{\mathrm{ac}}). \tag{45}$$

Similarly, for $\Delta I_{2A} - \Delta I_{2B}$

$$\frac{\Delta I_{2A} - \Delta I_{2B}}{E_2^{\text{read}}} \approx -(\Delta y_{\text{iBA}} - \Delta y_{\text{iBB}}) - (W^{\text{read}} + 1)(y_{\text{CB}} - y_{\text{ac}}). \quad (46)$$

Substituting (45) and (46) into (42) finally yields

$$\frac{\Delta W^{\text{sw}}}{W^{\text{read}}} \approx -\frac{R_3 Z_1}{R_3 + Z_1 + R_4 + Z_2}(\Delta y_{\text{iAA}} - \Delta y_{\text{iAB}}) - \frac{R_4 Z_2}{R_3 + Z_1 + R_4 + Z_2}(\Delta y_{\text{iBA}} - \Delta y_{\text{iBB}}) - \frac{Z_2(R_3 + R_4)}{R_3 + Z_1 + R_4 + Z_2}(W^{\text{read}} - 1)(y_{\text{CB}} - y_{\text{ac}}). \quad (47)$$

As can be seen from the above equation, the error depends on the asymmetries of the multiplexer between the two positions, and it is expected to increase proportionally to the measurement frequency due to the capacitive nature of the stray admittances.

C. Low Unbalance

If the bridge is imperfectly balanced with $V_{\text{LP1}} \neq 0$ and $V_{\text{LP2}} \neq 0$, errors like those analyzed in Section III-D arise. The voltages across the impedances Z_1 and Z_2 differ from E_1 and E_2, and the currents crossing Z_1 and Z_2 are not equal. Consequently, the effect of a low unbalance on W for a measurement without impedance swapping is given by (26), with impedance swapping by (28).

VI. Evaluating the Uncertainty and Choosing the Balancing Parameters

The analyses of Sections III and V can be exploited to evaluate the measurement uncertainty of an impedance ratio, optimize the bridge parameters for a specified target uncertainty, or correct certain systematic errors.

For the evaluation of the uncertainty, it should be first noted that all the quantities involved in the foregoing analyses are complex quantities, and the evaluation of the uncertainty should be performed according to [28]. This can be done by propagating the distributions of the complex quantities by means of a Monte Carlo method [29] or with the help of dedicated software packages, such as `Metas.UncLib` [30], which implements the propagation of uncertainty according to [31] and [28].

The uncertainty of an impedance ratio can be evaluated from the measurement models

$$W = W^{\text{read}} - \Delta W^{\text{nl}} - \Delta W^{\text{ct}} - \Delta W^{\text{ld}} - \Delta W^{\text{lb}} - \Delta W^{\text{hb}}, \quad \text{(generating)} \quad (48)$$

$$W = W^{\text{read}} - \Delta W^{\text{nl}} - \Delta W^{\text{sw}} - \Delta W^{\text{lb}}. \quad \text{(digitizing)}. \quad (49)$$

We should distinguish two cases[6]: single measurement and repeated measurements.

[6]The two cases can be likely unified into one by a Bayesian evaluation of the uncertainty.

In the case of a single measurement, the terms ΔW^{lb} and ΔW^{hb} in (48) and (49) can be evaluated in either of two ways as type B uncertainty components. In the first way, by considering that the bridge balancing algorithms usually stop when the magnitudes of the signals at the various detection points fall below certain thresholds predefined by the operator, this allows one to define uncertainty regions (usually circular or rectangular) for the quantities V_{LP}, ΔV_{LP}, I_{DHP1}, and I_{DHP2} (or V_{DHP1} and V_{DHP2}). In the second way, by monitoring the residual values of these quantities, in this case, the measured value can be corrected for the imperfect balance, and the uncertainty regions for V_{LP}, ΔV_{LP}, I_{DHP1}, and I_{DHP2} (or V_{DHP1} and V_{DHP2}) can be estimated from the noise associated with these signals.

In the case of repeated measurements, the terms $\Delta W^{\text{lb}} + \Delta W^{\text{hb}}$ in (48) and ΔW^{lb} in (49) contribute instead to the type A uncertainty of W^{read} and should, thus, be removed from the type B uncertainty components.

Finally, for given impedances Z_1 and Z_2, and given excitation current, the equations for ΔW^{nl}, ΔW^{ct}, ΔW^{sw}, ΔW^{lb}, and ΔW^{hb} allow the designer to find maximum limits on the bridge parameters g_k's and a_{kj}'s and on the balancing parameters V_{LP}, ΔV_{LP}, I_{DHP1}, and I_{DHP2} (or V_{DHP1} and V_{DHP2}) to achieve the desired target uncertainty.

VII. Characterization of Some Bridge Designs

The analyses of Sections III and V are here applied, as an example, to the preliminary characterization of the digital impedance bridges, both generating and digitizing, that are being developed within the framework of the project EMPIR 17RPT04 VersICaL.

The generating bridges, which are being developed by the Istituto Nazionale di Ricerca Metrologica (INRIM) and the National Standards Authority of Ireland (NSAI), are based on the seven-channel polyphase sinusoidal digital signal generator designed and manufactured by the University of Zielona Góra (UZG). This generator comes in two versions (DSS1 and DSS2A), and different units were shipped to some of the institutes involved in the project. In the following, the different units are labeled DSS1-INRIM, DSS2A-INRIM, DSS2A-NSAI, and DSS2A-UZG. The output frequency range of the generator is 20 Hz–20 kHz, and there are four available voltage ranges: 1 V, 2.5 V, 5 V, and 10 V. A picture of the INRIM bridge is shown in Fig. 3.

The digitizing bridge tested here is being developed by Trescal A/S and is based on a National Instrument NI PXI 4461 dynamic signal acquisition board as a digitizer and on a generator developed by the Silesian University of Technology [32]. A picture of this bridge is shown in Fig. 4.

Other characterizations of digitizers and generators can be found in [22], [23], and [32]–[34].

A. Generator Nonlinearity

The estimation of the bridge nonlinearity error through (7) requires the knowledge of the coefficients g_k's or, equivalently, Δg_k's from (10). These coefficients depend on the frequency, amplitude, and phase of the generated waveforms

Fig. 3. Picture of the generating bridge developed at the Istituto Nazionale di Ricerca Metrologica.

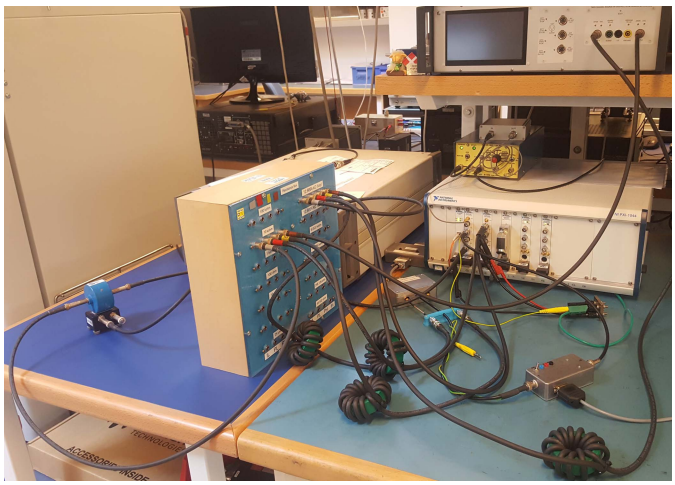

Fig. 4. Picture of the digitizing bridge developed at Trescal A/S.

and should be determined with respect to their fundamental components. The required coefficients can be measured by various methods: 1) comparison with a known voltage or impedance ratio; 2) permuting capacitor [35], [36] or build-up [37] methods; and 3) waveform recording by means of an accurate digitizer. It should be remarked, though, that the results obtained with different methods might not be comparable in a straightforward way because of possible differences in the measurand definition: not all methods allow the realization of the four-terminal pair definition, and some methods may not determine the nonlinearity with respect to the

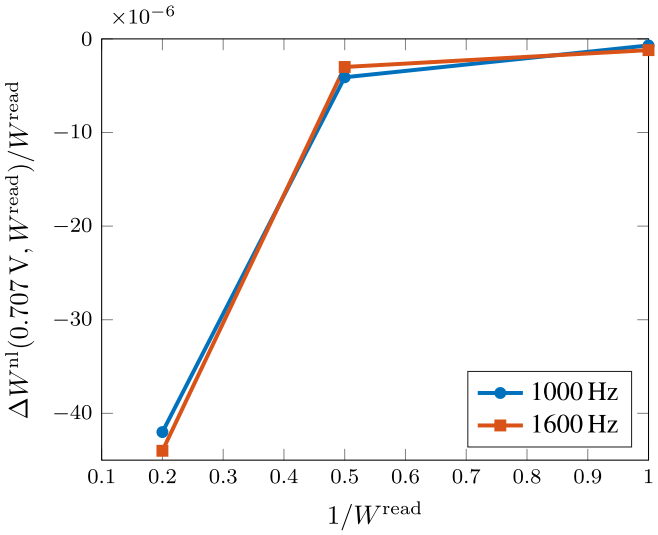

Fig. 5. Nonlinearity error of the generator DSS1-INRIM between channels 1 and 4 measured by comparison with a reference capacitance ratio for $E_{1\mathrm{F}}^{\mathrm{read}} \approx 0.707\,\mathrm{V}$ (rms).

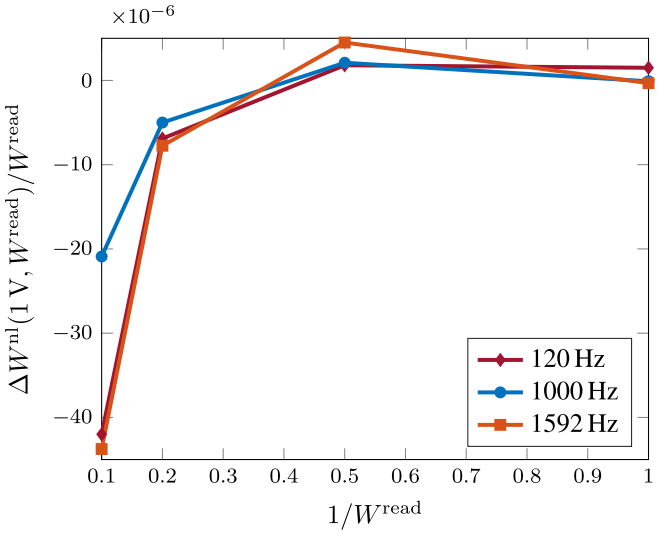

Fig. 6. Nonlinearity error of the generator DSS2A-UZG between channels 1 and 2 measured by comparison with an IVD for $E_{1\mathrm{F}}^{\mathrm{read}} \approx 1\,\mathrm{V}$ (rms).

fundamental component of the signals (see the last example in the following).

Fig. 5 reports, at 1 kHz and 1.6 kHz, the nonlinearity error of the generator DSS1-INRIM, between channels 1 and 4, measured by comparison with a reference capacitance ratio (2 nF : 2 nF, 1 nF : 2 nF, and 1 nF : 5 nF), obtained by an Andeen–Haegerling AH2700 ultraprecision capacitance bridge with nonlinearity at the 10^{-6} level. The measurement has been taken with $E_{1\mathrm{F}}^{\mathrm{read}} \approx 0.707\,\mathrm{V}$ (rms). During the measurement, the other sources of uncertainty have been kept below the 10^{-6} level.

Fig. 6 reports, at 120 Hz, 1 kHz, and 1.592 kHz, the nonlinearity error of the generator DSS2A-UZG, between channels 1 and 2, measured by comparison with the voltage ratio defined by an inductive voltage divider (IVD). The measurement has

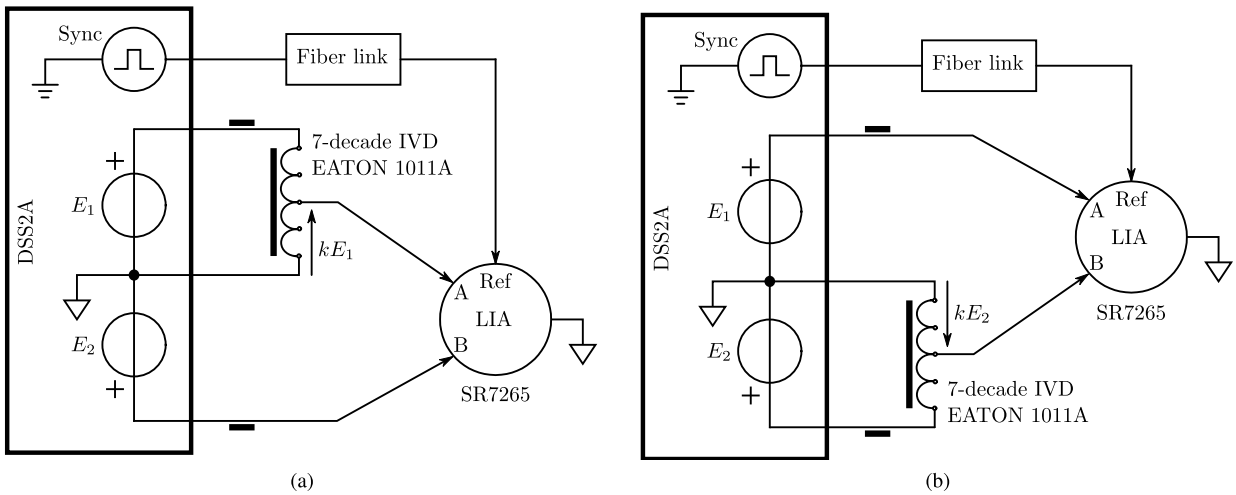

Fig. 7. Principle schematics for the nonlinearity measurements reported in Fig. 6 on the DSS2A-UZG generator: (a) forward and (b) reverse configurations; LIA represents a lockin amplifier with differential inputs A and B, and reference input Ref; IVD is an IVD.

been taken with $E_{1F}^{\text{read}} \approx 1\,\text{V}$ (rms). Fig. 7(a) (forward) and (b) (reverse) shows the measurement principle: the lock-in amplifier LIA measures the small voltage differences $V_{\text{ABF}} = kE_1 - E_2$ (forward) and $V_{\text{ABR}} = E_1 - kE_2$ (reverse), where $k = 1/W$ is defined by the IVD; the nonlinearity error is then obtained as

$$\frac{\Delta W^{\text{nl}}}{W^{\text{read}}} \approx -\frac{1}{2}\left(\frac{V_{\text{ABF}}}{E_{2F}^{\text{read}}} - \frac{V_{\text{ABR}}}{E_{1R}^{\text{read}}}\right). \tag{50}$$

This method cancels the common mode rejection ratio error of the lock-in amplifier since it is the same in the two configurations.

Finally, Fig. 8(a) reports the coefficients Δg_k's measured on the generator DSS2A-NSAI at 159 Hz and with $E_{\text{k}}^{\text{read}} \approx 0.707\,\text{V}$ (rms). The measurement was performed by digitizing the generated waveforms with a Keysight 3458A voltmeter and then by computing the rms value with the windowed discrete rms method [38], [39], with the Blackman–Harris window. Fig. 8(b) reports, for each possible channel pairing, the generator nonlinearity error calculated with (9), starting from the data of Fig. 8(a). This allows one to choose the channel pair minimizing the nonlinearity error [red line in Fig. 8(b)]. However, by comparing the values of Fig. 8(b) with those of Fig. 6 (different units, but the same type of generator), one can notice that those of the latter are generally smaller. The main reason is that the results of Fig. 8 are obtained with respect to the rms values of the waveforms and not with respect to the fundamental components. Since the bridge is balanced at the fundamental component, this discrepancy means that the characterization of the generator nonlinearity, that of interest for bridge measurements, should be performed with respect to the fundamental components of the generator output voltages and not with respect to their overall rms values.

B. Digitizer Nonlinearity

Fig. 9 reports, at 997 Hz and for $E_1^{\text{read}} \approx 1\,\text{V}$ (rms), the nonlinearity error of the digitizer NI PXI 4461, calculated with (34) from measurements obtained with the method described in [40]. The results of Fig. 9 are consistent with other characterizations of the NI PXI 4461 found in the literature [18], [33].

TABLE I

MAGNITUDE OF THE CROSSTALK COEFFICIENTS E_{10} AND a_{12} FOR THE DSS2A-INRIM GENERATOR ON THE 2.5 V RANGE AS A FUNCTION OF THE GENERATED FREQUENCY

Frequency	$\lvert E_{10}\rvert$	$\lvert a_{12}\rvert$
1 kHz	160 nV	1.8×10^{-8}
10 kHz	540 nV	2.2×10^{-8}
20 kHz	640 nV	6.2×10^{-8}

C. Generator Crosstalk

Table I reports the crosstalk coefficients E_{10} and a_{12} for the DSS2A-INRIM generator measured on the 2.5 V range at 1 kHz, 10 kHz, and 20 kHz (similar values were obtained for the other channels).

The coefficient E_{10} was measured by connecting channel 1 to a lock-in amplifier with reference connected to channel 7, set for an output amplitude of 1 V. All other channels were set for zero output voltage. The magnitude of E_{10} is approximately proportional to the selected range.

To determine a_{12}, channel 2 was set to an rms voltage of 1 V, with all other conditions as earlier. The coefficient a_{12} was then determined from the variation of channel 1's output voltage with respect to E_{10}. Channel 2 was loaded with a 10 kΩ resistor.

As remarked in Section III-B, when $W \approx \pm 1$, there is a partial cancellation of the terms in a_{12} and a_{21}; in this case, with the values of Table I, the residual uncertainty due to E_{10} and, likewise, E_{20} would be of about 10^{-7} at 1 kHz for output voltages close to the full-scale range of 2.5 V.

D. Multiplexer Switching

As discussed in Section V-B, the switching error depends on several stray admittances, one of which is the one between the ports of the multiplexer in the two positions.

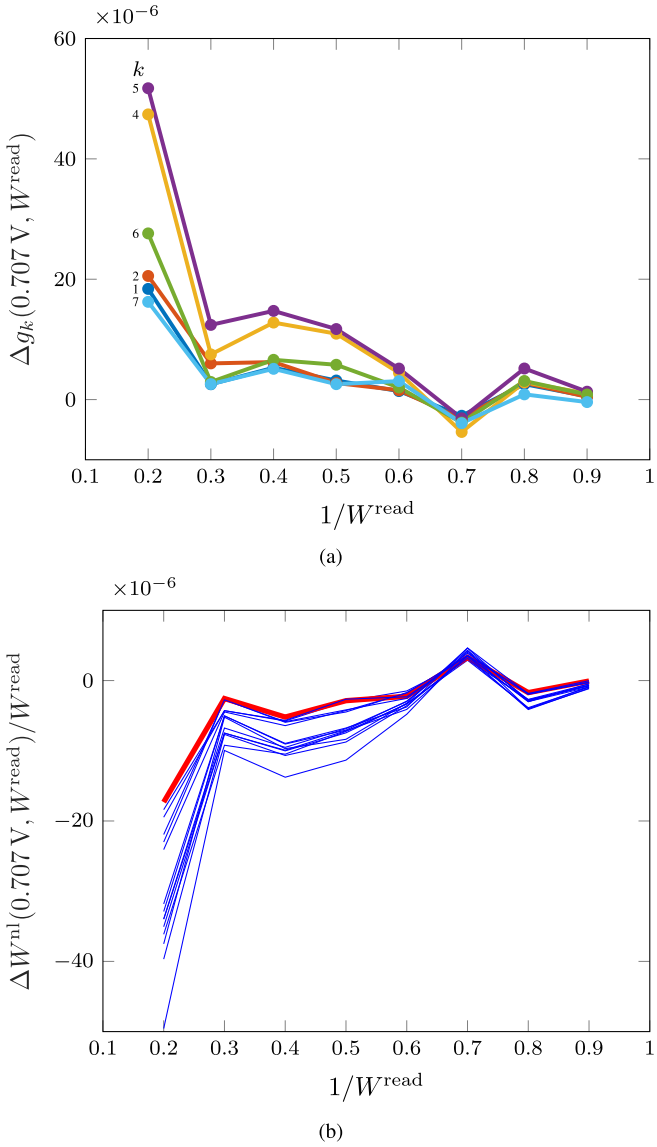

Fig. 8. Nonlinearity error of the generator DSS2A-NSAI at 159 Hz and $E_{1F}^{\text{read}} \approx 0.707$ V (rms), measured by digitizing the waveforms with a Keysight 3458A voltmeter and then by computing the rms value with the windowed discrete rms method. (a) Coefficients Δg_k's. (b) Generator nonlinearity error calculated with (9). The red line marks the channel pairing (channels 1 and 7), which minimizes the nonlinearity error at higher W ratios.

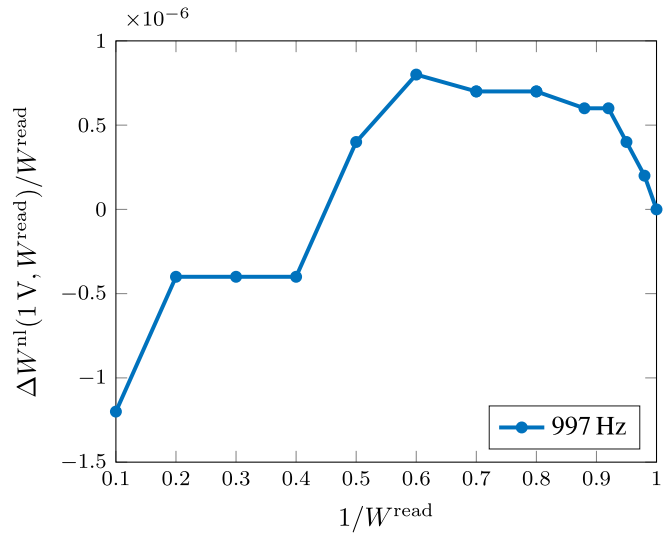

Fig. 9. Nonlinearity error of the digitizer NI PXI 4461 for $E_1^{\text{read}} \approx 1$ V (rms).

TABLE II
MULTIPLEXER CROSSTALK COEFFICIENTS FOR DIFFERENT PORT LOADING AND FREQUENCIES

Frequency	a_{21} (100 Ω load)	a_{21} (1000 Ω load)
1 kHz	$1.9 \times 10^{-8} + 6.4\text{j} \times 10^{-7}$	$2.7 \times 10^{-6} + 4.9\text{j} \times 10^{-6}$
10 kHz	$2.6 \times 10^{-6} + 5.0\text{j} \times 10^{-6}$	$1.1 \times 10^{-5} + 2.4\text{j} \times 10^{-6}$
16 kHz	$4.7 \times 10^{-6} + 6.0\text{j} \times 10^{-6}$	$1.1 \times 10^{-5} + 1.8\text{j} \times 10^{-6}$

Table II reports the crosstalk coefficients, as a function of frequency, measured on the multiplexer of the Trescal A/S bridge. These have been measured by applying a signal E_1 to port A of the multiplexer and measuring, with the digitizer, the signal V_2 at port B, with port B being loaded with a 100 Ω or 1000 Ω resistor, $a_{21} = V_2/E_1$. From these data, we can infer that the stray admittance y_{ac}, which was defined in Section V-B as the stray admittance between ports A and C when MUX is in position B, is a capacitance of about 1 pF.

E. Low Unbalance

To test the validity of (28), we performed seven repeated measurements with the INRIM generating bridge, comparing a 1 kΩ resistor and a 100 mH inductor with a high value (10 mV) of the balance threshold for V_{LP}. The threshold for ΔV_{LP} was set to 1 μV (usual value for this measurement).

Fig. 10(a) reports, in the complex plane, 14 recorded values for V_{LP} during the series of measurements: seven for the forward [V_{LPF} in (28)] and seven for the reverse configuration [V_{LPR} in (28)]. Fig. 10(c) shows a zoomed-in view of Fig. 10(a) around the center. The blue circles in Fig. 10(a) and (c) represent the bounds for the values of V_{LPF} and V_{LPR}.

Fig. 10(b) reports, in the complex plane, the deviations of the seven results, determined by combining forward and reverse measurements with (2), with respect to their average value $\bar{W}^{\text{read}}$. Fig. 10(d) shows a zoomed-in view of Fig. 10(b) around the center. The red circles in Fig. 10(b) and (d) represent the *worst case* bounds for $W^{\text{read}} - \bar{W}^{\text{read}}$ predicted from the bound of Fig. 10(a) and (c) through (28). All the measurements fall within the predicted bounds.

F. High Unbalance

As discussed in Section III-E, the measurement error caused by an imperfect balance at ports DHP1 and DHP2 depends on the residual signals at these ports, the channel output impedances of the generator, and the characteristics of the detection transformers T_1 and T_2.

For what concerns the channel output impedances, we should distinguish two cases, depending on whether the channel output has an additional series resistance or not. In the former case, which is common in commercial generators,

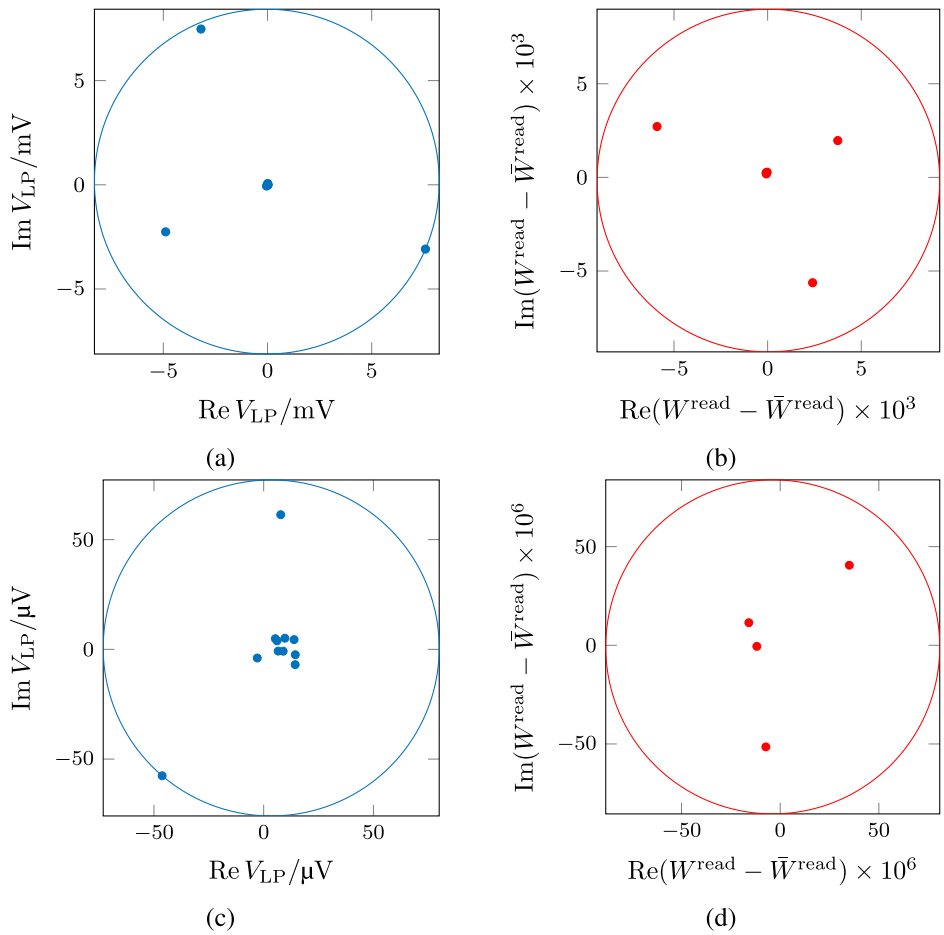

Fig. 10. Measurements performed on the INRIM generating bridge to test the validity of (28) (see Section VII-E). (a) Recorded complex values of V_{LP} during a series of seven measurements; (b) complex deviations of the seven results with respect to their average; (c) zoomed-in view of (a) around the center; (d) zoomed-in view of (b) around the center. The blue circles in (a) and (c) represent the bounds for the values of V_{LPF} and V_{LPR}. The red circles in (b) and (d) represent the worst case bounds for $W^{read} - \bar{W}^{read}$ predicted from the bounds of (a) and (c).

or when the measurand impedances are high capacitances (see footnote 4), the output resistance is typically from a few ohms to a few tens of ohm. In the latter, the output resistance is that of a high-current buffer that can be typically modeled as a resistance (typically, tens of milliohm) in series with an inductance (typically, a few microhenries or less). In this case, the error from the high unbalance is frequently well below the 10^{-6} level, even at high balance thresholds.

For what concerns the type of detection, current detection is typically better at low-current levels because the lock-in amplifier easily overloads at high-current levels. When used as low-current detectors, lock-in amplifiers typically have input resistances of the order of 1 kΩ. When used as voltage detectors, lock-in amplifiers typically have an input impedance dominated by the input capacitance in parallel with the capacitance of the cable connecting the lock-in amplifier to the detection point. In both types of detection, one should consider the effect of the lock-in amplifier loading on the detection transformers.

In the INRIM generating bridge, T_1 and T_2 are 1 : 200 transformers. In current-detection mode, the lock-in input impedance does not load significantly the transformers, and one can use $n \approx 200$ in (32). In voltage-detection mode, the mutual impedance Z_m mainly depends on the mutual inductance of the transformers, but the lock-in amplifier loading is no longer negligible. We measured $Z_m \approx (87 - 160i)$ Ω at 1000 Hz and $Z_m \approx (205 - 275i)$ Ω at 1541 Hz. The values of the imaginary part correspond to a mutual inductance of about 25 mH.

VIII. Conclusion

The error analysis herewith presented is intended as a tool useful both in the design of digital bridges, by allowing an informed choice of the bridge topology and components, and during its operation, to calculate corrections to the bridge readings and evaluate the measurement uncertainty.

The modeling presented allows one to analyze both generating and digitizing bridges, providing a uniform approach for deriving the error terms for both bridge types. The influence of the different error sources on the measurement outcome is strongly dependent on the bridge type, specific properties of the components employed, and the values of the standards being compared. As a rule of thumb, generating bridges might be more suitable for the comparison of high-valued impedances, for which even the simplified two-terminal pair version [8] can be sufficiently accurate. Digitizing bridges

might be more appropriate for low-valued impedance comparisons since the digitizer is less sensitive to the increasing distortion of the generator. In digitizing bridges, a simplified four-terminal definition [41], [42] can also be appropriate.

The application of the analysis to the different bridges and the measurements performed in the framework of the EMPIR 17RPT04 VersICaL project confirm the generality of the approach and provide examples for further applications by the interested readers.

References

[1] F. Overney and B. Jeanneret, "Impedance bridges: From Wheatstone to Josephson," *Metrologia*, vol. 55, no. 5, pp. S119–S134, Oct. 2018.

[2] G. Trenkler, "Digitalmeßbrücke zum vergleich von wirk-und blindwiderständen," *Technisches Messen*, vols. 503–513, 1978.

[3] H. Bachmair and R. Vollmert, "Comparison of admittances by means of a digital double-sinewave generator," *IEEE Trans. Instrum. Meas.*, vol. 29, no. 4, pp. 370–372, Dec. 1980.

[4] W. Helbach, P. Marczinowski, and G. Trenkler, "High-precision automatic digital AC bridge," *IEEE Trans. Instrum. Meas.*, vol. 32, no. 1, pp. 159–162, Mar. 1983.

[5] H. Schollmeyer, "A digital AC bridge as an impedance to frequency converter," *IEEE Trans. Instrum. Meas.*, vol. IM-34, no. 3, pp. 389–392, Sep. 1985.

[6] W. Helbach and H. Schollmeyer, "Impedance measuring methods based on multiple digital generators," *IEEE Trans. Instrum. Meas.*, vol. IM-36, no. 2, pp. 400–405, Jun. 1987.

[7] F. Overney and B. Jeanneret, "RLC bridge based on an automated synchronous sampling system," *IEEE Trans. Instrum. Meas.*, vol. 60, no. 7, pp. 2393–2398, Jul. 2011.

[8] L. Callegaro, V. D'Elia, M. Kampik, D. B. Kim, M. Ortolano, and F. Pourdanesh, "Experiences with a two-terminal-pair digital impedance bridge," *IEEE Trans. Instrum. Meas.*, vol. 64, no. 6, pp. 1460–1465, Jun. 2015.

[9] W. G. K. Ihlenfeld and R. T. B. Vasconcellos, "A digital four terminal-pair impedance bridge," in *Conf. Precis. Electromagn. Meas. (CPEM)*, Ottawa, ON, Canada: IEEE, Jul. 2016, pp. 1–2.

[10] J. Kučera and J. Kováč, "A reconfigurable four terminal-pair digitally assisted and fully digital impedance ratio bridge," *IEEE Trans. Instrum. Meas.*, vol. 67, no. 5, pp. 1199–1206, May 2018.

[11] M. Ortolano *et al.*, "An international comparison of phase angle standards between the novel impedance bridges of CMI, INRIM and METAS," *Metrologia*, vol. 55, no. 4, pp. 499–512, Aug. 2018.

[12] J. Schurr, V. Bürkel, and B. P. Kibble, "Realizing the farad from two AC quantum Hall resistances," *Metrologia*, vol. 46, no. 6, pp. 619–628, Dec. 2009.

[13] L. Callegaro, V. D'Elia, and B. Trinchera, "Realization of the farad from the DC quantum Hall effect with digitally assisted impedance bridges," *Metrologia*, vol. 47, no. 4, pp. 464–472, Aug. 2010.

[14] F. Overney *et al.*, "Josephson-based full digital bridge for high-accuracy impedance comparisons," *Metrologia*, vol. 53, no. 4, pp. 1045–1053, Aug. 2016.

[15] S. Bauer *et al.*, "A novel two-terminal-pair pulse-driven Josephson impedance bridge linking a 10 nF capacitance standard to the quantized Hall resistance," *Metrologia*, vol. 54, no. 2, pp. 152–160, Apr. 2017.

[16] T. Hagen, L. Palafox, and R. Behr, "A Josephson impedance bridge based on programmable Josephson voltage standards," *IEEE Trans. Instrum. Meas.*, vol. 66, no. 6, pp. 1539–1545, Jun. 2017.

[17] F. Overney *et al.*, "Dual Josephson impedance bridge: Towards a universal bridge for impedance metrology," *Metrologia*, vol. 57, no. 6, Dec. 2020, Art. no. 065014.

[18] F. Overney and B. Jeanneret, "Realization of an inductance scale traceable to the quantum Hall effect using an automated synchronous sampling system," *Metrologia*, vol. 47, no. 6, pp. 690–698, Dec. 2010.

[19] M. Ortolano *et al.*, "Error sources in electronic fully-digital impedance bridges," in *Conf. Precis. Electromagn. Meas. (CPEM)*, Aug. 2020, pp. 1–2.

[20] *VersICaL Joint Research Project Homepage*. [Online]. Available: https://sites.google.com/inrim.it/versical/home

[21] S. Awan, B. Kibble, and J. Schurr, *Coaxial Electrical Circuits for Interference-Free Measurements* (Electrical Measurement Series). Edison, NJ, USA: IET, 2011.

[22] J. Kučera, J. Kováč, L. Palafox, R. Behr, and L. Vojáčková, "Characterization of a precision modular sinewave generator," *Meas. Sci. Technol.*, vol. 31, no. 6, Jun. 2020, Art. no. 064002.

[23] M. Kozioł, J. Kaczmarek, and R. Rybski, "Characterization of PXI-based generators for impedance measurement setups," *IEEE Trans. Instrum. Meas.*, vol. 68, no. 6, pp. 1806–1813, Jun. 2019.

[24] P. Symons, *Digital Waveform Generation*. Cambridge, U.K.: Cambridge Univ. Press, 2014.

[25] S. Franco, *Design With Operational Amplifiers and Analog Integrated Circuits*, 4th ed. New York, NY, USA: McGraw-Hill, 2014.

[26] H. W. Ott, *Electromagnetic Compatibility Engineering*. Hoboken, NJ, USA: Wiley, 2009.

[27] J. Kucera, T. Funck, and J. Melcher, "Automated capacitance bridge for calibration of capacitors with nominal value from 10 nF up to 10 mF," in *Conf. Precis. Electromagn. Meas.*, Jul. 2012, pp. 596–597.

[28] BIPM, IEC, IFCC, ILAC, ISO, IUPAC, IUPAP, and OIML. (2011). *Evaluation of Measurement Data—Supplement 2 to the 'Guide to the Expression of Uncertainty in Measurement'—Extension to Any Number of Output Quantities, JCGM 102:2011*. [Online]. Available: https://www.bipm.org/en/publications/guides/gum.html

[29] BIPM, IEC, IFCC, ILAC, ISO, IUPAC, IUPAP, and OIML. (2008). *Evaluation of Measurement Data—Supplement 1 to the 'Guide to the Expression of Uncertainty in Measurement'—Propagation of Distributions Using a Monte Carlo Method, JCGM 101:2008*. [Online]. Available: https://www.bipm.org/en/publications/guides/gum.html

[30] M. Zeier, J. Hoffmann, and M. Wollensack, "Metas.UncLib—A measurement uncertainty calculator for advanced problems," *Metrologia*, vol. 49, p. 809, 2012.

[31] BIPM, IEC, IFCC, ILAC, ISO, IUPAC, IUPAP, and OIML, "Evolution of the 'Guide to the Expression of Uncertainty in Measurement,'" *JCGM* 100:2008, 2008. [Online]. Available: https://www.bipm.org/en/publications/guides/gum.html

[32] M. Kampik and K. Musioł, "Investigations of the high-performance source of digitally synthesized sinusoidal voltage for primary impedance metrology," *Measurement*, vol. 168, Jan. 2021, Art. no. 108308.

[33] F. Overney, A. Rufenacht, J.-P. Braun, B. Jeanneret, and P. S. Wright, "Characterization of metrological grade Analog-to-Digital converters using a programmable Josephson voltage standard," *IEEE Trans. Instrum. Meas.*, vol. 60, no. 7, pp. 2172–2177, Jul. 2011.

[34] M. Kampik, "Analysis of the effect of DAC resolution on AC voltage generated by digitally synthesized source," *IEEE Trans. Instrum. Meas.*, vol. 63, no. 5, pp. 1235–1243, May 2014.

[35] R. D. Cutkosky and J. Q. Shields, "The precision measurement of transformer ratios," *IRE Trans. Instrum.*, vol. I-9, no. 2, pp. 243–250, Sep. 1960.

[36] J. Kučera, R. Sedlaáček, and J. Boháček, "A new capacitance device for calibration of N: 1 HF inductive voltage dividers," in *Conf. Precis. Electromagn. Meas. (CPEM)*. Daejeon, South Korea: IEEE, Jun. 2010, pp. 390–391.

[37] N. T. M. Tran, V. D'Elia, L. Callegaro, and M. Ortolano, "A capacitance build-up method to determine LCR meter errors and capacitance transfer," *IEEE Trans. Instrum. Meas.*, vol. 69, no. 8, pp. 5727–5735, Aug. 2020.

[38] R. Lapuh, B. Voljc, and M. Lindic, "Measurement and estimation of arbitrary signal power using a window technique," in *Conf. Precis. Electromagn. Meas. (CPEM)*, Jul. 2016, pp. 1–2.

[39] R. Lapuh, *Sampling With 3458A: Understanding, Programming, Sampling and Signal Processing*. Ljubljana, Slovenia: Left Right, 2018.

[40] L. Callegaro, V. D'Elia, and F. Manta, "A setup for linearity measurement of precision ac voltmeters in the audio frequency range," in *Proc. 16th IMEKO TC4 Symp.*, Florence, Italy, Sep. 2008, pp. 15–19.

[41] L. Callegaro, V. D'Elia, and E. Gasparotto, "Impedance comparison at power frequency by asynchronous sampling," in *Conf. Precis. Electromagn. Meas. (CPEM)*, Jun. 2010, pp. 322–323.

[42] R. Rybski, J. Kaczmarek, and M. Kozioł, "A PXI-based calibration system for low-value AC resistors," *IEEE Trans. Instrum. Meas.*, vol. 67, no. 4, pp. 905–911, Apr. 2018.

Massimo Ortolano was born in 1969. He received the M.Sc. degree in electronic engineering and the Ph.D. degree in metrology from the Politecnico di Torino, Turin, Italy, in 1997 and 2001, respectively.

Since 2000, he has been an Assistant Professor with the Department of Electronics and Telecommunications, Politecnico di Torino, where he is in charge of several courses about electronic measurements. Since 2006, he has been collaborating with the Istituto Nazionale di Ricerca Metrologica (INRIM), Turin, on noise metrology, modeling of quantum Hall effect devices, and impedance metrology. His research interests include also fundamental constants, time and frequency metrology, and statistical methods for the evaluation of the uncertainty.

Martina Marzano was born in 1989. She received the master's degree in physics from the Università di Torino, Turin, Italy, in 2016, and the Ph.D. degree for her research on novel devices and methods for quantum resistance and impedance metrology from the Politecnico di Torino, Turin, in 2020, in collaboration with the Istituto Nazionale di Ricerca Metrologica (INRIM), Turin.

From 2018 to 2019, she was a Guest Researcher with the National Institute of Standards and Technology, Gaithersburg, MD, USA, for six months. As a Post-Doctoral Fellow with the working group of Quantum Metrology and Nano Technologies Division, INRIM, her current research at INRIM is focused on the development and modeling of quantum Hall effect devices and measurement methods for impedance metrology.

Vincenzo D'Elia was born in 1965. He received the High School degree in electronics from the Technical School G. Plana, Turin, Italy, in 1988.

In 1996, he joined the Department of Electrical Metrology, Istituto Nazionale di Ricerca Metrologica, Turin, where he is currently with the Division of Quantum Metrology and Nano Technologies. His current research interests include impedance, inductive voltage ratio, and low-current measurements.

Ngoc Thanh Mai Tran was born in Ho Chi Minh City, Vietnam, in 1992. She received the B.Sc. and M.Sc. degrees in electronic engineering from the Politecnico di Torino, Turin, Italy, in 2014 and 2017, respectively. She is currently pursuing the Ph.D. degree in metrology with the Politecnico di Torino and the Istituto Nazionale di Ricerca Metrologica, Turin.

She did her master's thesis at the National Metrology Institute of Japan (NMIJ), Tsukuba, Japan. She is currently a Guest Researcher with the Korea Research Institute of Standards and Science (KRISS), Daejeon, South Korea. She is involved in several projects related to the metrology of electrical resistance and impedance.

Ryszard Rybski (Member, IEEE) received the M.Sc. degree in electrical engineering from the University of Zielona Góra, Zielona Góra, Poland, in 1979, the Ph.D. degree from the Wrocław University of Technology, Wrocław, Poland, in 1989, and the Habilitate Doctorate (D.Sc.) degree from the University of Zielona Góra in 2008.

Since 1979, he has been with the Faculty of Computer, Electrical and Control Engineering, Institute of Metrology, Electronics and Computer Science, University of Zielona Góra, where he became the Director in 2008 and the University Professor in 2010. His research interests include high-accuracy measurements of electrical quantities, in particular with precision impedance measurements.

Janusz Kaczmarek (Member, IEEE) received the M.Sc. and Ph.D. degrees in electrical engineering and the Habilitate Doctorate (D.Sc.) degree in automation, electronic, and electrical engineering from the University of Zielona Góra, Zielona Góra, Poland, in 1989, 1996, and 2020, respectively.

He is currently an Assistant Professor with the Institute of Metrology, Electronics and Computer Science, University of Zielona Góra. He is a supervisor and a main researcher of many research projects for the industry. His areas of interest include precision electrical measurements, instrumentation and virtual instrumentation, and embedded hardware and software design.

Mirosław Kozioł (Member, IEEE) received the M.Sc. degree in electrical engineering from the Technical University of Zielona Góra, Zielona Góra, Poland, in 1998, and the Ph.D. degree from the University of Zielona Góra, Zielona Góra, in 2006.

Since 1998, he has been with the Faculty of Computer, Electrical and Control Engineering, Institute of Metrology, Electronics and Computer Science, University of Zielona Góra, where he is currently an Assistant Professor. His current research interests include precision impedance metrology, digital signal processing, and software design for embedded systems.

Krzysztof Musioł was born in Katowice, Poland, in 1977. He received the M.Sc. and Ph.D. degrees in electrical engineering from the Silesian University of Technology, Gliwice, Poland, in 2002 and 2007, respectively.

He has been a Lecturer with the Institute of Electrical Measurements, Silesian University of Technology, since 2007. His current research interests include the development of calibration facilities in impedance measurements.

Dr. Musioł is also a member of the Polish Association of Theoretical and Applied Electrotechnics.

Andreas Elmholdt Christensen received the B.Sc. and M.Sc. degrees in physics with a specialization in experimental physics from Aarhus University, Aarhus, Denmark, in 2008 and 2011, respectively

In 2011, he joined the Danish AC Electrical Standards Laboratory, Department of Trescal A/S, Silkeborg, Denmark. His research interests include digital sampling systems, measurements of impedance, ac power, and power quality.

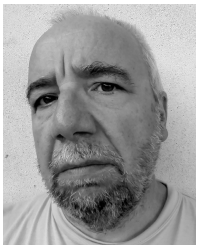

Luca Callegaro was born in 1967. He received the M.Sc. degree in electronic engineering and the Ph.D. degree in physics from the Politecnico di Milano, Milan, Italy, in 1992 and 1996, respectively.

He joined the Istituto Nazionale di Ricerca Metrologica (INRIM), Turin, Italy, in 1996, where he is currently the Head of the Quantum Electronics Group. He is also responsible for the Italian National standards of electrical capacitance, inductance, ac resistance, and ac voltage ratio. He has authored about 100 articles on international reviews and the book *Electrical Impedance: Principles, Measurement and Applications* (Taylor & Francis, 2012). His research interest is focused on electrical impedance metrology.

Dr. Callegaro is a member, and served four years as the Chair, of the Technical Committee for Electricity and Magnetism (TC-EM) of EURAMET, the European Association of National Metrology Institutes, and the Italian delegate to the Consultative Committee for Electricity and Magnetism (CCEM) of the International Committee for Weights and Measures (CIPM).

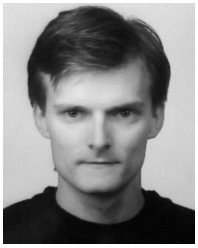

Jan Kucera was born in 1980. He received the M.Sc. degree in measurement and instrumentation and the Ph.D. degree in measurement techniques from the Department of Measurements, Faculty of Electrical Engineering (FEE), Czech Technical University in Prague (CTU), Prague, Czech Republic, in 2005 and 2012, respectively.

Since 2007, he has been an Assistant Professor with the Department of Measurements, FEE, CTU. From 2008 to 2011, he was involved in research on quantum impedance metrology with the Physikalisch-Technische Bundesanstalt, Brunswick, Germany. In 2011, he joined the Czech Metrology Institute, Brno, Prague, where he is engaged in primary metrology of dc resistance and electrical impedance quantities.

Oliver Power (Member, IEEE) received the B.Sc. and M.Sc. degrees in experimental physics from the University College Cork, Cork, Ireland, in 1978 and 1981, respectively, and the Ph.D. degree from the Dublin Institute of Technology, Dublin, Ireland, in 2006.

He is a Technical Manager with the National Standards Authority of Ireland, where he is responsible for the development, maintenance, and dissemination of the Irish national measurement standards for electrical quantities. His research interests include the characterization of electronic voltage standards and the evaluation of measurement uncertainty.